MADRID
inter.noise 2019
June 16 - 19
NOISE CONTROL FOR A BETTER ENVIRONMENT

Study of analytical and numerical models for diffuse field sound absorption prediction according to the porous panel dimensions

Mareze, Paulo Henrique[1]
Federal University of Santa Maria, Structure and building department, Acoustics Engineering
Av. Roraima, n. 1000, 97105-900, Santa Maria, RS, Brazil

Pereira, Matheus[2]
Godinho, Luís[3]
Amado Mendes, Paulo[4]
ISISE, Dep Civil Engineering, University of Coimbra
Rua Luís Reis Santos, Pólo 2 da Universidade de Coimbra, 3030-788 Coimbra, Portugal

ABSTRACT

There are many doubts about the proper calculation of the sound absorption coefficient of the porous materials when applied in a room, under diffuse field. The simple use of impedance tube data for this purpose (according to ISO 10534-2, [1]) is not entirely correct since it considers only incident plane waves. There are several diffuse-field sound absorption calculations in the literature, but many of them cannot realistically approximate the measured data in the reverberant chamber, according to ISO 354, [2]. The most interesting approach considers the exact finite dimensions of the absorbent panel within the room but the calculation isn't clear. The current work deals with the possibilities of calculation and prediction of diffuse field sound absorption. For this purpose, saound absorption data have been obtained up to 5 kHz from literature. Two-dimensional finite and boundary element methods that consider the angle of sound incidence and refraction inside the material will also be approached as an alternative simulation. At the end, comparisons between reverberant chamber results and the cited models are made. Different porous panel dimensions are evaluated using the validated model.

Keywords: Porous materials characterization, sound absorption, diffuse field, impedance tube, reverberation room
I-INCE Classification of Subject Number: 35
(see http://i-ince.org/files/data/classification.pdf)

[1]paulo.mareze@eac.ufsm.br
[2]matheus.pereira@student.dec.uc.pt
[3]lgodinho@dec.uc.pt
[4]pamendes@dec.uc.pt

1. INTRODUCTION

Nowadays, the correct characterization of porous absorbers and resonators is very important for a great final result. Many industries or companies lack information on the acoustic characteristics of absorbent materials. Manufacturers usually present sound absorption data in octave bands, obtained experimentally, without further information. However, when the acoustic designer needs to perform finite element or acoustic ray analysis, it would be valuable to have more detailed information, allowing a careful choice of the material to be used. Often the designer does not have direct access to the materials or enough area to carry out a reverberant chamber test. Sometimes, when working with new materials or combinations, some have used impedance tube data, since only small samples are needed. However, it is known that such results are not valid for a diffuse field sound environment, as is the case for example in common rooms such as a theater or auditorium.

For the designer or acoustic engineer, it would be quite useful to have access to a reliable simulation model that could allow accurately extracting the sound absorption of a reverberant chamber without expensive measurements, but only using input data obtained from simpler impedance tube measurement, such as surface impedance for normal incidence, or even better, complex wave number and complex density on the frequency domain. From these data, one can use inverse methods for extracting macroscopic parameters; alternatively, when small samples are available, the two-cavity, two-thickness or three microphones methods are also practical and do not require additional acoustics instrumentation (for further details, see [3], [4] and [5]).

Another issue is the possibility to test changes in shapes, curvatures, differentiated surfaces, bass traps among others. In fact, it is useful to be able to obtain and use the correct coefficients for the exact panel dimensions in the acoustic model of a room. One can then verify how the diffuse field sound absorption changes with the panel area or shape of the absorber panel.

Some empirical and theoretical models are available with different levels of accuracy. The intention of this work is to evaluate different strategies of estimating the diffuse field sound absorption coefficient, testing them for the case of a single and uniform layer of material (melamine foam). The next sections intend to present the mathematics fundamentals which form the bases of the analytical and numerical approaches. Then, some results are presented and discussed.

2. FUNDAMENTALS

The first approach to be presented is based on the oblique acoustic plane wave solution including incidence and refraction inside a simple porous absorber layer, like an equivalent fluid. In the second approach, a very similar strategy is applied, but making use of a 2D finite element model to extract the surface impedance and associated refraction effects inside the material for every oblique plane wave incidence, between normal and grazing angles. Both are decoupled to the external air medium, but consider the impedance radiation effects of the finite sample edges to recover the coupling and the correct diffuse absorption. The third approach is the complete solution of a 3D boundary element model that couples the internal porous material to an external air medium. Here the radiation impedance is already physically included when the incident sound power and the sample sound power absorption of a finite size of single porous layer are

calculated.

2.2.1. Analytical oblique acoustic plane wave

According to [6], the surface impedance of a single porous layer, assuming plane wave oblique incidence, can be calculated as Equation 1,

$$\tilde{Z}_{\mathrm{s}}(\theta_i) = -\mathrm{j}\frac{\tilde{Z}_c}{\cos(\theta_t)}\cot\left[\tilde{k}_c\cos(\theta_t)\,d\right], \tag{1}$$

that depends on the oblique incidence angle and transmitted angle, which can be found using the Snell-Descartes law [7], given by Equation 2,

$$\theta_t = \arcsin[(k_0/\tilde{k}_c)\sin(\theta_i)], \tag{2}$$

in which the air characteristic impedance is Z_0 and the wavenumber is $k_0 = 2\pi f/c_0$. Observing the porous absorber side, the complex equivalent wavenumber in the porous material is $\tilde{k}_c$ and the complex characteristic impedance is $\tilde{Z}_c$, which can be obtained from the complex Bulk Modulus, $\tilde{K}_{\mathrm{eq}}$, and equivalent fluid density of the porous material, $\tilde{\rho}_{\mathrm{eq}}$.

The representation of wave incidence and wave refraction inside the porous layer can be seen in Figure 1. Here, d is the thickness of the porous sample, being infinite on the horizontal plane.

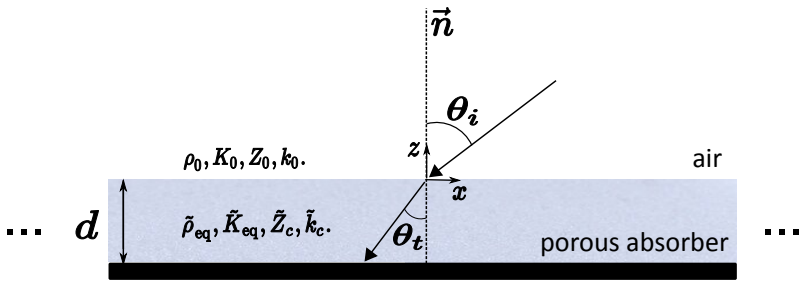

Figure 1: Oblique plane wave incidence over an infinite porous absorber.

The analytical model assumes that the layers are infinite in the lateral directions (x axis). Therefore, the resulting prediction tends to be biased relative to measurements registered with samples of finite size. To account for this effect, the influence of the radiation impedance of the finite sample is included in the calculation. A single equivalent fluid layer of rectangular dimension is represented in Figure 2, where the elevation and azimuth angles of plane wave incidence, (θ_i, ϕ), are also represented.

The normalized radiation impedance seen by the finite rectangular absorber can be calculated as in Equation 3 (for more details, please see [8], [9], [10] and [11]),

$$\frac{\tilde{Z}_{\mathrm{rad}}(\theta_i,\phi)}{Z_0} = \frac{\mathrm{j}k_0}{2\pi ab}\int_0^a\int_0^b 4\cos(k_0\mu_x\kappa)\cos\left(k_0\mu_y\tau\right)\frac{\mathrm{e}^{-jk_0\sqrt{\kappa^2+\tau^2}}}{\sqrt{\kappa^2+\tau^2}}(a-\kappa)(b-\tau)\mathrm{d}\kappa\mathrm{d}\tau. \tag{3}$$

This Equation 3 can be solved numerically through the Matlab's 2016 double integration function called "integral2(fun, 0, a, 0, b)". Some simplified equations for radiation impedance can be found in [12] and [13], but these were not evaluated in this work. The terms μ_x and μ_y are defined by $\mu_x = \sin(\theta_i)\cos(\phi)$, $\mu_y = \sin(\theta_i)\sin(\phi)$,

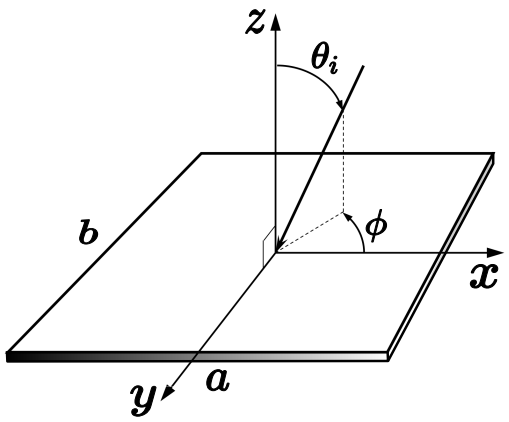

Figure 2: An incident wave impinging upon a single equivalent fluid layer of rectangular shape with dimensions $a \times b$. Adapted from [8].

respectively. The incident sound power over the sample area due to a plane wave incoming from a given direction in a 2D space (x-z plane) can be calculated as

$$\Pi_{\text{inc}}(\theta_i) = \frac{|\tilde{p}_{\text{inc}}|^2 \, ab}{2Z_0} \cos(\theta_i), \tag{4}$$

in which $\tilde{p}_{\text{inc}}$ is the complex amplitude of the incoming plane wave. Sources of real unitary amplitude can be applied for simplification. The impedance radiation effect due to the frame is not accounted, so the incident sound power considers an infinite free space (denoted by the subscript 'inf'). The radiation impedance is simply $\tilde{Z}_{\text{rad}} = Z_0/\cos(\theta_i)$.

Specifically, the diffuse field absorption coefficient for any elevation or azimuth angle is calculated as $\alpha(\theta_i, \phi) = \Pi_{\text{abs}}/\Pi_{\text{inc}}$. The absorbed sound power by a porous sample of infinite dimension in terms of free space radiation impedance is

$$\Pi_{\text{abs,inf}}(\theta_i) = \frac{|\tilde{p}_{\text{inc}}|^2 \, ab}{2Z_0} \left(\frac{4 \, \text{Re}\left(\frac{\tilde{Z}_s(\theta_i)}{Z_0}\right)}{\left|\frac{\tilde{Z}_s(\theta_i)}{Z_0} + \frac{1}{\cos(\theta_i)}\right|^2} \right), \tag{5}$$

in which ab is the surface area portion where the absorbed sound power was calculated. On the other hand, the absorbed sound power carried out by a finite porous sample must consider the exact tridimensional radiation impedance, $\tilde{Z}_{\text{rad}}(\theta_i, \phi)$, and it is calculated by Equation 6,

$$\Pi_{\text{abs,fin}}(\theta_i, \phi) = \frac{|\tilde{p}_{\text{inc}}|^2 \, ab}{2Z_0} \left(\frac{4 \, \text{Re}\left(\frac{\tilde{Z}_s(\theta_i)}{Z_0}\right)}{\left|\frac{\tilde{Z}_s(\theta_i)}{Z_0} + \frac{\tilde{Z}_{\text{rad}}(\theta_i,\phi)}{Z_0}\right|^2} \right). \tag{6}$$

Applying the trapezoidal rule of numerical integration for 90° elevation and 360° azimuth angles, it is possible to find the incident and absorbed sound power. The common term $|\tilde{p}_{\text{inc}}|^2 \, ab/2Z_0$ can be simplified and the diffuse field absorption coefficient due to an infinite porous sample is

$$\alpha_{\text{inf}} = \frac{\int_0^{2\pi} \int_0^{\pi/2} \Pi_{\text{abs,inf}}(\theta_i) \sin(\theta_i) \text{d}\theta_i \text{d}\phi}{\int_0^{2\pi} \int_0^{\pi/2} \Pi_{\text{inc}}(\theta_i) \sin(\theta_i) \text{d}\theta_i \text{d}\phi} = \frac{\int_0^{\pi/2} \alpha(\theta_i) \cos(\theta_i) \sin(\theta_i) \, \text{d}\theta_i}{\int_0^{\pi/2} \cos(\theta_i) \sin(\theta_i) \, \text{d}\theta_i}. \tag{7}$$

The oblique absorption coefficient, in this case, is $\alpha(\theta_i) = 4\,\mathrm{Re}\left(\frac{\tilde{Z}_s(\theta_i)}{Z_0}\right) / \left|\frac{\tilde{Z}_s(\theta_i)}{Z_0} + \frac{1}{\cos(\theta_i)}\right|^2$. The diffuse field absorption coefficient due to a finite porous layer can be evaluated as

$$\alpha_{\mathrm{fin}} = \frac{\int_0^{2\pi}\int_0^{\pi/2} \Pi_{\mathrm{abs,fin}}(\theta_i, \phi)\sin(\theta_i)\mathrm{d}\theta_i\mathrm{d}\phi}{\int_0^{2\pi}\int_0^{\pi/2} \Pi_{\mathrm{inc}}(\theta_i)\sin(\theta_i)\mathrm{d}\theta_i\mathrm{d}\phi}. \tag{8}$$

Apparently, Equation 8 can well represent the absorption of a rectangular porous sample measured inside a reverberant chamber over diffuse field (please, see [8]). Numerical approaches are going to be proposed in the next section.

3. METHODOLOGY

In this section, two approaches are presented to estimate the diffuse field sound absorption of a porous sample. Although the analytical model is an interesting way of solving the problem, it is limited to flat surfaces of rectangular shape. So, two numerical approaches are here proposed which may allow overcoming this limitation. The first proposal is a bi-dimensional finite element model decoupled of the external medium/air, while the second is a three-dimensional boundary element model with a coupling between the porous material and the external air medium. These two methodologies may allow geometrical changes in the surface of the sample, and indeed the three-dimensional BEM model may allow to model any shape or size.

3.3.1. Finite element model - FEM 2D

An equivalent 2D porous layer can be represented by a finite element model (FEM) considering the complex bulk modulus, $\tilde{K}_{\mathrm{eq}}(\omega)$, and equivalent fluid density, $\tilde{\rho}_{\mathrm{eq}}(\omega)$. The elementary finite element mass and stiffness are presented in Equation 9 and Equation 10, respectively,

$$\mathbf{Q}^{\mathrm{e}}_{\mathrm{i,j}} = \frac{1}{\tilde{K}_{\mathrm{eq}}(\omega)} \int_{\zeta_1}\int_{\zeta_2} N_{\mathrm{i}}\left(\zeta_1, \zeta_2\right) N_{\mathrm{j}}\left(\zeta_1, \zeta_2\right) \det(\mathrm{J})\mathrm{d}\zeta_2\mathrm{d}\zeta_1, \tag{9}$$

$$\mathbf{H}^{\mathrm{e}}_{\mathrm{i,j}} = \frac{1}{\tilde{\rho}_{\mathrm{eq}}(\omega)} \int_{\zeta_1}\int_{\zeta_2} \left[\mathrm{J}^{-1}\nabla N_{\mathrm{i}}\left(\zeta_1, \zeta_2\right)\right]^{\mathrm{T}} \left[\mathrm{J}^{-1}\nabla N_{\mathrm{j}}\left(\zeta_1, \zeta_2\right)\right] \det(\mathrm{J})\mathrm{d}\zeta_2\mathrm{d}\zeta_1, \tag{10}$$

in which the linear shape functions are N_{i} and N_{j}. For further details, see references [14] and [15]. The term J is the Jacobian matrix of the local/global coordinates transformation. After the elementary assembling procedure, the dynamic movement equation is

$$\left[\mathbf{H} - \omega^2\mathbf{Q}\right]\{\tilde{p}\} = -\mathrm{j}\omega\{\tilde{q}\}, \tag{11}$$

that can be solved using a direct method. In that equation, $\{\tilde{q}\}$ is the nodal force vector representing the acoustic volume velocity of the sources. Considering a plane wave oblique incidence (see Figure 3) the volume velocity loading over the surface nodes (red points) was calculated for 90° elevation angles, $[0, \pi/2]$.

The refraction effect is already physically represented by the FEM model and the normal surface impedance, $\tilde{Z}_s(\theta_i)$, was evaluated for all the surface nodes, and a mean value was taken for each frequency. This FEM procedure approach only replaces the analytical surface impedance shown in Equation 1. All subsequent procedures for considering the finite sample size and impedance radiation effect to couple the external

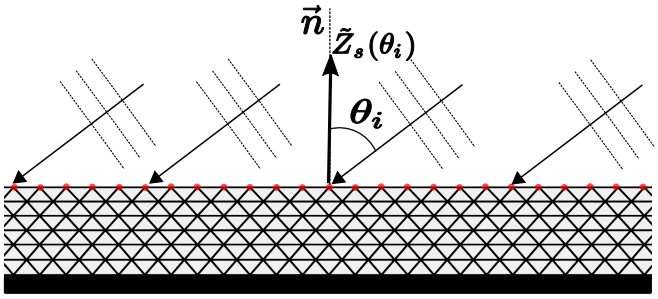

Figure 3: Decoupled finite porous absorber represented by FEM 2D. The red points represent the nodal acoustic velocity due to the oblique plane wave incidence over the surface. The horizontal x axis dimension is $a = 4$ [m].

medium were accounted through the analytical equations already mentioned (Equation 3 to Equation 7).

3.3.2. Boundary element model - BEM 3D

This classic formulation of the Boundary Element Method (BEM) can include the coupling between the external air and the internal porous medium, and it allows the simulation and study of any type of geometry, incorporating the associated shape effects. In addition, the effects of radiation impedance are already automatically recovered and any analytical correction of this term is required.

A residual or weak integral formulation together with the Green's function for the test function leads to the Kirchhoff–Helmholtz integral equation as (for further details, see ref. [16] and [17]),

$$c_p \tilde{p}\left(\mathbf{x}_0\right) = -\mathrm{j}\rho\omega \sum_{j=1}^{N_{be}} \tilde{v}(\mathbf{x}, \vec{n}) \int_{\Gamma_j} G\left(\mathbf{x}, \mathbf{x}_0\right) \mathrm{d}\Gamma_j - \sum_{j=1}^{N_{be}} \tilde{p}(\mathbf{x}) \int_{\Gamma_j} H\left(\mathbf{x}, \mathbf{x}_0, \vec{n}\right) \mathrm{d}\Gamma_j + \tilde{p}_{\mathrm{inc}}\left(\mathbf{x}_0, \mathbf{x}_{\mathrm{s}}\right), \tag{12}$$

in which $\mathbf{x}_0$ represents the center coordinate of the boundary element *be* above the surface Γ_j. The terms $\mathbf{x}$ and $\mathbf{x}_{\mathrm{s}}$ represent the boundary nodes and sources coordinates, respectively. It can be condensed using a matrix form as

$$\mathrm{j}\omega\rho\mathbf{G}\tilde{\mathbf{v}} + \mathbf{H}\tilde{\mathbf{p}} - 0.5\mathbf{I}\tilde{\mathbf{p}} = \tilde{\mathbf{p}}_{\mathrm{inc}}. \tag{13}$$

In this case, the acoustic boundary integral equation is set up for the inner and outer field, respectively. Combined with normal acoustic pressure and particle velocity continuity on the surface, the integral equation can be expressed as (see [18], [19])

$$\begin{cases} j\omega\rho_0\mathbf{G}_{\mathrm{air}}\{\tilde{v}\} + \mathbf{H}_{\mathrm{air}}\{\tilde{p}\} = \{\tilde{p}_{\mathrm{inc}}\} \\ -\mathrm{j}\omega\tilde{\rho}_{\mathrm{eq}}\mathbf{G}_{\mathrm{por}}\{\tilde{v}\} + \mathbf{H}_{\mathrm{por}}\{\tilde{p}\} = 0 \end{cases}, \tag{14}$$

or then,

$$\begin{bmatrix} \mathrm{j}\omega\rho_0\mathbf{G}_{\mathrm{air}} & \mathbf{H}_{\mathrm{air}} \\ -\mathrm{j}\omega\tilde{\rho}_{\mathrm{eq}}\mathbf{G}_{\mathrm{por}} & \mathbf{H}_{\mathrm{por}} \end{bmatrix} \begin{Bmatrix} \tilde{v} \\ \tilde{p} \end{Bmatrix} = \begin{Bmatrix} \tilde{p}_{\mathrm{inc}} \\ 0 \end{Bmatrix}. \tag{15}$$

Here, the terms $\mathbf{H}_{\mathrm{air}}$ and $\mathbf{H}_{\mathrm{por}}$ must account the $-0.5\mathbf{I}$ part that comes from the collocation constant, c_p. The solution is found by direct Gauss elimination of the equation system. Recovering the acoustic pressure and particle velocity throughout the

boundary surface, the external acoustic pressure at field points with coordinates $\mathbf{x}_{\text{fp}}$ can be calculated from

$$\tilde{p}\left(\mathbf{x}_{\text{fp}}\right) = -\text{j}\rho\omega \sum_{j=1}^{N_{be}} \tilde{v}(\mathbf{x_0}, \vec{n}) \int_{\Gamma_j} G\left(\mathbf{x_0}, \mathbf{x}_{\text{fp}}\right) \text{d}\Gamma_j - \sum_{j=1}^{N_{be}} \tilde{p}(\mathbf{x_0}) \int_{\Gamma_j} H\left(\mathbf{x_0}, \mathbf{x}_{\text{fp}}, \vec{n}\right) \text{d}\Gamma_j + \tilde{p}_{\text{inc}}\left(\mathbf{x}_{\text{fp}}, \mathbf{x}_{\text{s}}\right). \tag{16}$$

To find the sound power absorbed by the porous sample, $\Pi_{\text{abs,bem}}$, according to [20], the numerical integration can be performed directly over the boundary surface of the porous material, S, as presented on Equation 17,

$$\Pi_{\text{abs,bem}} = \frac{1}{2}\,\text{Re}\left[\int_S \tilde{p}\tilde{v}_n^* dS\right] \approx \frac{1}{2}\,\text{Re}\left[\sum_{j=1}^{N_{be}} \tilde{p}(\mathbf{x_0})\tilde{v}_n^*(\mathbf{x_0}) S_j\right], \tag{17}$$

where the surface pressure, $\tilde{p}$, and the complex conjugate of the normal surface velocity, $\tilde{v}_n^*$, are used to find the absorbed power. A large number of real point sources (62248 sources) were distributed in an 1/8th of a sphere (positive x, y, z quadrant). All the sources are used at the same time and are positioned in a radius of 60 meters from the sample center coordinate (their effect is almost that of a group of plane waves). These sources have unit pressure and are equally spaced, trying to represent the dispersion caused by a complete reverberant field.

The incident sound power, $\Pi_{\text{inc,free}}$, is evaluated using the fundamental wave solution, from Green's function. A finite difference of the pressure over the boundary area, or p-p method, was used to calculate the incident sound intensity, $I_{\text{inc}}(\omega) \approx -\text{Im}\left[\tilde{p}_1 \cdot \tilde{p}_2^*\right]/2\rho_0\omega\Delta d$, in which $\Delta d = 0.001$ [m] is the p-p spacing (more details in [21], [22]). The incident power in free field space evaluated over the sample surface without any porous material is $\Pi_{\text{inc,free}} = \sum_{j=1}^{N_{be}} I_{\text{inc}\,j} S_j$. The diffuse field absorption coefficient is $\alpha_{\text{bem}} = \Pi_{\text{abs, bem}}/\Pi_{\text{inc, free}}$. A boundary element mesh of a sample with 60 [mm] tick and lateral sides $a = 4$ [m], $b = 3$ [m] is shown in Figure 4.

This internal/external coupled model is symmetric on $x = 0$ and $y = 0$ planes. The plane $z = 0$ represent the rigid floor where the sample is supported. Those symmetry planes were used here to prevent computational cost and reduce simulation time.

3.3.3. Experiments

Some important details are presented here about the performed experiments. The diffuse field experiments were carried out following the recommendations from [2] and [23]. The results were presented by BASF (Basotect®, G+) and can be seen at [24]. The normal incidence measurement is presented in [25] and it was done by BASF according to [1].

The computational analyses were made to normal and diffuse sound incidence of a melamine foam with 60 mm thick and top area of 4x3 m^2. All the macroscopic parameters were measured using direct methods and some details can be found in [26] and [27].

The macroscopic parameters used with the JCAL-Limp model are flow resistivity, $\sigma = 12,1$ [kNs/m^4], porosity, $\phi = 0,98$, tortuosity, $\alpha_\infty = 1,00$, characteristics lengths, $\Lambda = 115$ [μm], $\Lambda = 116$ [μm], total apparent density, $\rho_t = 9,6$ [kg/m^3]. The statical thermal permeability considered here is $k_0' = 1.51\text{x}10^{-9}$ [m^2].

The impedance tube standard [1] proposes a simplified calculation based on London's equation to estimate the diffuse field absorption using the normal incidence impedance

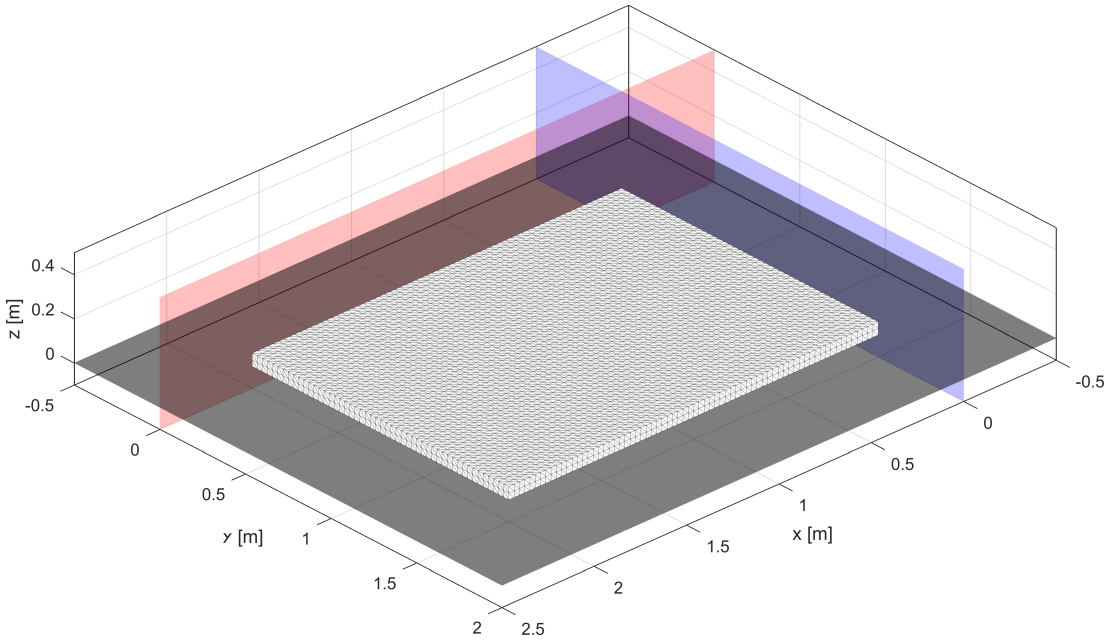

Figure 4: Example of boundary element mesh of a porous layer with $a = 4$ [m] and $b = 3$ [m] over a rigid floor (gray) and symmetry planes (red and blue).

tube data, $\tilde{Z}_n$. The calculation only considers infinite sample size and the propagation inside the material is locally reacting (normal transmission and no refraction).The calculation procedure is depicted in Equation 18,

$$\alpha_d = 8\gamma_n \left\{1 - \gamma_n \ln\left[r'/\gamma_n + 2r' + 1\right] + \left(x'/r'\right)\gamma_n \left(\left(r'/x'\right)^2 - 1\right)\arctan\left(x'/\left(r' + 1\right)\right)\right\}, \quad (18)$$

in which, $\gamma_n = r'/\left(r'^2 + x'^2\right)$, $r' = \mathrm{Re}[\tilde{Z}_n/\rho_0 c_0]$ and $x' = \mathrm{Im}[\tilde{Z}_n/\rho_0 c_0]$. On the other hand, from the normal incidence sound absorption, α_n, in the 50's Albert London found two simple empirical equations, called the first and second London's models. According to [28] and [29], they are, respectively,

$$\alpha_b = 8\left[\frac{1 - \sqrt{1 - \alpha_n}}{1 + \sqrt{1 - \alpha_n}}\right]^2 \left[\frac{2}{1 - \sqrt{1 - \alpha_n}} - \frac{1 - \sqrt{1 - \alpha_n}}{2} + 2\ln\left(\frac{1 - \sqrt{1 - \alpha_n}}{2}\right)\right], \quad (19)$$

and

$$\alpha_s = 4\left[\frac{1 - \sqrt{1 - \alpha_n}}{1 + \sqrt{1 - \alpha_n}}\right]\left[\ln\left(\frac{2}{1 - \sqrt{1 - \alpha_n}}\right) - \frac{1 + \sqrt{1 - \alpha_n}}{2}\right]. \quad (20)$$

4. RESULTS

Some test results are presented in this section. First, a comparison between impedance tube measurements (for the case of normal incidence), analytical results, FEM 2D and BEM 3D models is presented (see Figure 5(a)) . Observing this figure, a good agreement can be seen between all models and the experimental data, with only a small deviation occurring at around 2.5 kHz between the experimental and the calculated results. The boundary element model was run only up to 640 Hz, due to memory and computational time problems.

In the sequence, Figure 5(b) shows a comparison between several analytical approaches to estimate the diffuse field sound absorption of the sample. All the tests were carried out for elevation incidence angle in the range $\theta_i = [0, \pi/2]$. The three models based on London's work are presented in comparison with experimental reverberation room measurements. Clearly, using the analytical model that considers a locally reacting sample of infinite size leads to a erroneous absorption curve compared with the measured sample, as also occurs for the ISO 10534-2 method. The first and second empirical models proposed by London can provide a better representation of the shape of the measured curve, but present quite reduced absorption coefficients, with a difference up to 0.16 [-]. The analytical finite size model, considering the radiation impedance effect ($\theta_i = [0, \pi/2]$ and $\phi = [0, 2\pi]$) for $a = 4$ [m] and $b = 3$ [m] could reproduce the measured result very well, as was expected. It is clearly seen that the worst prediction case was from London's ISO 10534-2 and the edge radiation effect in fact must be accounted to obtain better results.

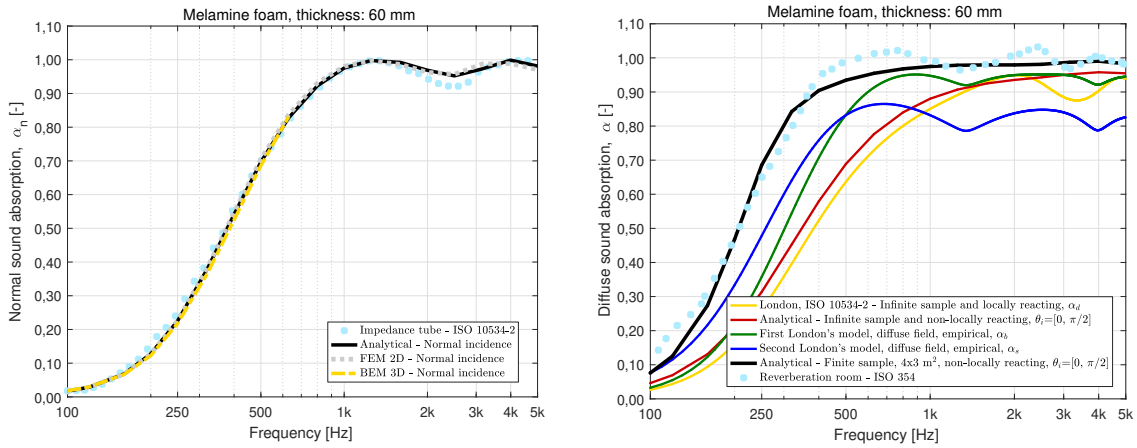

(a) Normal incidence

(b) Diffuse incidence and London's models

Figure 5: Normal incidence modeling comparison with impedance tube (a) and reverberation room diffuse incidence comparison with London's and analytical models (b).

To verify the validity of the analytical model, two approaches were proposed, one using the proposed finite element model and the other using the boundary element method. The comparison results between the numerical modeling and experiment can be observed in Figure 6(a).

The presented results reveal a very good agreement, although some differences are found above 1 kHz with respect to the BEM 3D (which can be due to the mesh size). Again, computational memory was a limitation to analyze higher frequencies using the BEM. The FEM 2D mesh was defined using 20 elements per wavelength ($f_{\max} = 5$ kHz) and the BEM 3D mesh using 12 elements per wavelength ($f_{\max} = 1$ kHz). Using a Intel Xeon® CPU processor, model E3-1240 v5 3.50 GHz, with 16 GB of RAM, each frequency step takes 11 minutes (255 seconds to assembly matrices and 376 seconds to solve) to run the in-house developed BEM 3D model with 9386 triangular elements and 4819 nodes. Some parts of the code use parallel processing connected to 4 working cores.

The last result (see Figure 6(b)) is an analytical prediction of the effect of the sample size . It is possible to see, that considering infinite size for diffuse field incidence, leads to a very low absorption coefficient compared to the ISO 354 measurement. But,

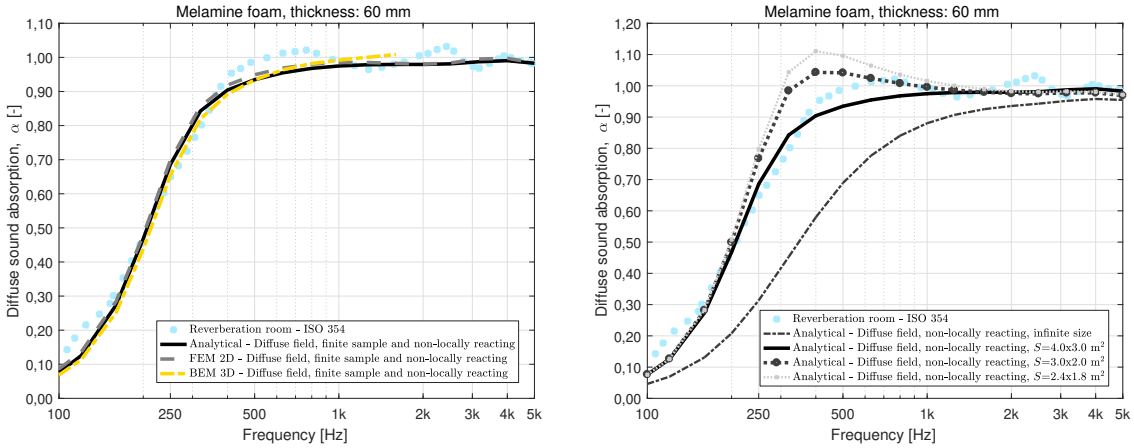

(a) Diffuse incidence with finite size

(b) Sample size effect

Figure 6: Diffuse incidence comparison (a) and sample size effects due to radiation impedance (b).

in fact, the decrease of the sample's surface area leads to progressively higher values, and even exceeds the measured result and the maximum unitary scale for a theoretical total absorption. A visible peak occurs at 400 Hz considering this type of material and thickness of 60 mm.

The fact that some reverberant room measurements are made with smaller, joined sample sizes may cause inter-laboratory deviations in the amplitude of the measured absorption.

5. CONCLUSIONS

In this work, the authors presented analytical and numerical modeling to predict the coefficient of absorption of melamine samples measured according to ISO 354 standard [2], in reverberant room. The proposed numerical methodology considers a finite element model in two dimensions and the coupling of the radiation to the external medium is done by the radiation impedance calculated previously. A boundary element model is proposed in three dimensions, coupling the external medium with the porous material, directly accounting for all these effects. Physically, the model may be capable of solving any type of geometry in three dimensions. It is assumed that the FEM 2D model allows any variation of geometry, but only in the x-z plane.

It is important to emphasize that the correct sample size must be represented in order to obtain a satisfactory result. The fact of neglecting the internal refraction effects of the material can lead to some errors, especially for samples of low flow resistivity that tend to present non-locally reacting behavior. Therefore, according to [30], one might expect that samples with high flow resistivity can be considered as locally reactive.

The best of the tested empirical models was found to be the second London's equation, α_s. In addition, the diffuse locally reacting equation from ISO 10534-2 should be avoided, at least for materials with similar macroscopic properties and dimensions as the one presented in this paper.

6. ACKNOWLEDGEMENTS

The authors acknowledge gratefully the research grant under the Optimized Wood R&D project - 'Optimization of forest resources in construction', POCI-01-0247-FEDER-017867, funded by the European Regional Development Fund (FEDER) through the Operational Competitiveness and Internationalization Program (POCI). We also thank the support from ISISE group at University of Coimbra as well as FCTUC.

This work was also partly financed by FEDER funds through the Competitivity Factors Operational Programme - COMPETE and by national funds through FCT – Foundation for Science and Technology within the scope of the project POCI-01-0145-FEDER-007633 and through the Regional Operational Programme CENTRO2020 within the scope of the project CENTRO-01-0145-FEDER-000006.

The authors also acknowledge COST Action DENORMS CA15125, supported by COST (European Cooperation in Science and Technology).

7. REFERENCES

[1] ISO 10534-2: 2001. Acoustics-determination of sound absorption coefficient and impedance in impedance tubes-part 2: Transfer function method. *BS EN ISO*, pages 10534–2, 2001.

[2] ISO 354: 2003. Acoustics—measurement of sound absorption in a reverberation room. *British Standards Institution*, 2003.

[3] Hideo Utsuno, Toshimitsu Tanaka, Takeshi Fujikawa, and AF Seybert. Transfer function method for measuring characteristic impedance and propagation constant of porous materials. *The Journal of the Acoustical Society of America*, 86(2):637–643, 1989.

[4] Charles D Smith and Tony L Parrott. Comparison of three methods for measuring acoustic properties of bulk materials. *The Journal of the Acoustical Society of America*, 74(5):1577–1582, 1983.

[5] T. Iwase, Y. Izumi, and R. Kawabata. A new measuring method for sound propagation constant by using sound tube without any air spaces back of a test material. In *INTER-NOISE and NOISE-CON Congress and Conference Proceedings*, volume 1998, pages 1265–1268. Institute of Noise Control Engineering, 1998.

[6] E. Brandão. *Acústica de salas: projeto e modelagem*. Editora Blucher, 2018.

[7] R. Descartes. *Discourse on the Method*. Perennial Press, 2018.

[8] A. R. Allen, N. H. Schiller, et al. Experimental evaluation of equivalent-fluid models for melamine foam. In *INTER-NOISE and NOISE-CON Congress and Conference Proceedings*, volume 252, pages 511–521. Institute of Noise Control Engineering, 2016.

[9] S. Thomasson. On the absorption coefficient. *Acta Acustica united with Acustica*, 44(4):265–273, 1980.

[10] J. Brunskog. The forced sound transmission of finite single leaf walls using a variational technique. *The Journal of the Acoustical Society of America*, 132(3):1482–1493, 2012.

[11] N. H. Schiller and A. R. Allen. Tuned chamber core panel acoustic test results. 2016.

[12] M. Vercammen and M. Lautenbach. Influence of sample size on the sound absorption. *Proceedings DAGA, Darmstadt*, 2012.

[13] D. Larner and J. Davy. The prediction of the diffuse field sound absorption of perforated panel systems. In *Inter-Noise 2015: Implementing Noise Control Technology*, pages 1–12. Institute of Noise Control Engineering, 2015.

[14] N. Atalla and F. Sgard. *Finite element and boundary methods in structural acoustics and vibration*. CRC Press, 2015.

[15] G. Copetti, P. Mareze, F. Dresch, S. Margheti, A. Gomes, M. Monteiro, W. Fonseca, E. Brandao, and L. Specht. Modelagem em elementos finitos do campo acústico de um pneu sobre camadas porosas asfálticas. In *XXVIII Encontro da Sociedade Brasileira de Acústica*, 2018.

[16] S. Marburg. Boundary element method for time-harmonic acoustic problems. In *Computational Acoustics*, pages 69–158. Springer, 2018.

[17] L. Godinho. Perspetiva sobre a aplicação de métodos numéricos avançados em problemas acústicos exteriores. *Revista de acústica*, 49(3):3–11, 2017.

[18] L. Godinho. *Propagação de ondas em sistemas que requerem o estudo da interacção sólido-fluido*. PhD thesis, Coimbra University, 2004.

[19] M. Yang, Y. Ai, and S. Xiang. Coupling of fem and exterior/interior acoustic field with bem and numerical simulation of vibro-acoustic response of elastic target. In *2010 International Conference on Measuring Technology and Mechatronics Automation*, volume 1, pages 864–868. IEEE, 2010.

[20] J. Allard and N. Atalla. *Propagation of sound in porous media: modelling sound absorbing materials 2e*. John Wiley & Sons, 2009.

[21] J. Chung. Cross-spectral method of measuring acoustic intensity without error caused by instrument phase mismatch. *The Journal of the Acoustical Society of America*, 64(6):1613–1616, 1978.

[22] F. Fahy. Measurement of acoustic intensity using the cross-spectral density of two microphone signals. *The Journal of the Acoustical Society of America*, 62(4):1057–1059, 1977.

[23] ISO 3382: 2009. Acoustics—measurement of room acoustic parameters - part 1. *British Standards Institution*, 2009.

[24] Basf - sound absorption of basotect® g+ (reverberation room). https://www.plasticsportal.net/wa/plasticsEU~en_GB/portal/show/content/products/foams/basotect_popup/popup_basotect_18. Accessed: 2019-03-09.

[25] Basf - sound absorption of basotect® g+ (impedance tube). https://www.plasticsportal.net/wa/plasticsEU~en_GB/portal/show/content/products/foams/basotect_popup/popup_basotect_06. Accessed: 2019-03-09.

[26] P. Mareze, E. Brandão, W. Fonseca, O. M. Silva, and A. Lenzi. Modeling of acoustic porous material absorber using rigid multiple micro-ducts network: Validation of the proposed model. *Journal of Sound and Vibration*, 443:376–396, 2019.

[27] P. Mareze. Análise da influência da microgeometria na absorção sonora de materiais porosos de estrutura rígida. Federal University of Santa Catarina, 2013.

[28] A. London. The determination of reverberant sound absorption coefficients from acoustic impedance measurements. *The Journal of the Acoustical Society of America*, 22(2):263–269, 1950.

[29] F. Bécot and J. Rodenas. Predicting alpha cabin sound absorption in an industrial context. In *INTER-NOISE and NOISE-CON Congress and Conference Proceedings*, volume 253, pages 4648–4658. Institute of Noise Control Engineering, 2016.

[30] E. Brandão, P. Mareze, A. Lenzi, and A. R. da Silva. Impedance measurement of non-locally reactive samples and the influence of the assumption of local reaction. *The Journal of the Acoustical Society of America*, 133(5):2722–2731, 2013.